Hunting for QCD strings in e^+e^--annihilation.

M. E. Kozhevnikova
In collaboration with:
O. V.Teryaev
A. G. Oganesian

Joint Institute for Nuclear Research

Dubna, September 2018

Plan of the presentation

1. Operator product expansion and short strings.
2. The fitting of experimental data on e^+e^--annihilation to hadrons
3. PT and APT
4. Adler function and the Borel transform
5. Extraction of the power corrections in the OPE of D-function related to short strings. Corellation between short string and gluon condensate.
6. Conclusions

Introduction

Zakharov's short string[1] leads to the corrections in annihilation cross-section (or Adler function). In Cornell potential

$$V(r) \approx -\frac{4\alpha_s(r)}{3r} + kr$$

the second part kr describes short string potential and leads to the correction $\sim \frac{k}{Q^2}$, in OPE the first correction to e^+e^--annihilation cross-section is $\sim \frac{\langle G_{\mu\nu} G^{\mu\nu} \rangle}{Q^4}$.

$[k] = [M^2]$.

Our purpose is an accurate analysis of Adler function and search for existing correction with dimension 2.

[1] K.G. Chetyrkin, S. Narison, V.I. Zakharov, "Short-distance tachyonic gluon mass and $1/Q^2$ corrections", Nucl.Phys. B550 (1999) 353-374

Introduction

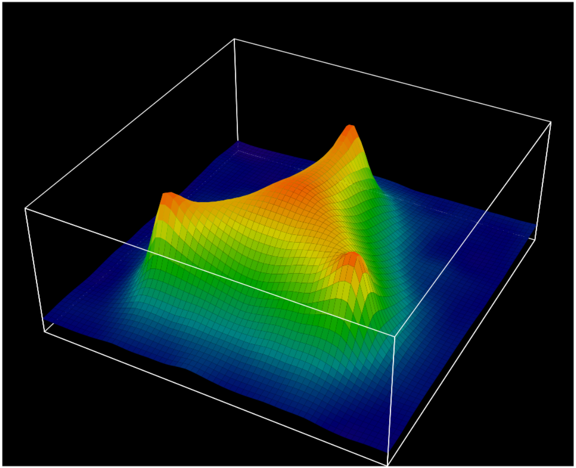

Fig.: String potential from lattice QCD (M.I. Polikarpov et al.)

Introduction

QCD description of e^+e^- -annihilation cross-section at low Q^2 . Operator product expansion and condensates. Gluon and quark condensate and corrections:

$$C_4 = \frac{2\pi^2}{3}\left\langle \frac{\alpha_s GG}{\pi} \right\rangle, \quad C_6 = \frac{448\pi^3}{27}\alpha_s \langle \bar{q}q \rangle^2 \approx -0.116\,\mathrm{GeV}^6$$

New condensate connected with Zakharov's short string is possible. Gluon field compose the string configuration and leads to confinement.

Construction of the model of the data

The using data is obtained on the detectors CMD, CMD-2, BaBar, SND, M3N, DM1, DM2, OLYA, GG2:

$$\begin{aligned}
e^+e^- &\to \pi^+\pi^- \text{ (CMD and OLYA detectors)},\\
e^+e^- &\to 2\pi^+2\pi^- \text{ (BaBar)},\\
e^+e^- &\to \pi^+\pi^-2\pi^0 \text{ (OLYA, CMD2, SND, DM2, Frascati-ADONE-GAM}\\
e^+e^- &\to 3\pi^+3\pi^- \text{ (BaBar)},\\
e^+e^- &\to 2\pi^+2\pi^-2\pi^0 \text{ (BaBar)}.
\end{aligned}$$

χ^2-functional:

$$\chi^2(a_1, \dots, a_d) = \frac{1}{N_{\text{d.f.}}} \sum_{n=1}^{N} \frac{\left(f_{\text{exp}}(s_n) - f_{\text{th}}(s_n; \{a_1, \dots, a_d\})\right)^2}{\delta f_{\text{exp}}(s_n)^2},$$

where $\{(s_i, f_{\text{exp}}(s_i))\}_{i=1,\dots,N}$ is an experimental points set, $f_{\text{th}}(s; \{a_1, \dots, a_d\})$ - the analytic function.

Construction of the model of the data

The 3-resonance model was used, the form factor of each resonance was calculated according to the Breit-Wigner model.

$$F^{\mathrm{BW}}(s, m_V, \Gamma_V) = \frac{m_V^2(1 + d \cdot \Gamma_V / m_V)}{m_V^2 - s + f(s, m_V, \Gamma_V) - i\, m_V \Gamma_V(s)} \,,$$

$$\text{where} \quad \Gamma_V(s) = \Gamma_V \left(\frac{k(s)}{k(m_V^2)} \right)^3, \quad k(s) = \frac{\sqrt{s - 4m_\pi^2}}{2} \,,$$

$$f(s, m_V, \Gamma_V) = \Gamma_V \frac{m_V^2}{k(m_V^2)^3} \left[k^2(s)(h(s) - h(m_V^2)) - (s - m_V^2) k^2(m_V^2) h'(m_V^2) \right],$$

$$h(s) = \frac{2}{\pi} \frac{k(s)}{\sqrt{s}} ln(\frac{\sqrt{s} + 2\, m_\pi}{2\, m_\pi}), \quad h'(m_V^2) = h'(s)\big|_{s=m_V^2} \,,$$

there $F^{\mathrm{BW}}(0, m_V, \Gamma_V) = 1$ automatically.
The resonances ρ, ω and ρ'.

Construction of the model of the data

For cross-sections of the processes $e^+e^- \to 2\pi^+2\pi^-$, $e^+e^- \to \pi^+\pi^-2\pi^0$, $e^+e^- \to 2\pi^+2\pi^-2\pi^0$, and $e^+e^- \to 3\pi^+3\pi^-$ the description in the form of sum of three Gaussian curves, describing wide resonances, is assumed:

$$F_{\text{Gauss}}\left(s, \{M_i, \sigma_i, \alpha_i\}\right) = \sum_{i=1}^{3} \alpha_i \, e^{-(\sqrt{s}-M_i)^2/(2\sigma_i^2)} \, ;$$

$$\sigma\left(s, \{M_i, \sigma_i, \alpha_i\}\right) [\text{nb}] = \theta(s - 4m_\pi^2) \, 0.3839 \cdot 10^6 \, F_{\text{Gauss}}^2 \, \frac{\pi \, \alpha_{em}}{3s} \, \left(1 - \frac{4m_\pi^2}{s}\right)^{3/2} \, .$$

Fitting. Results.

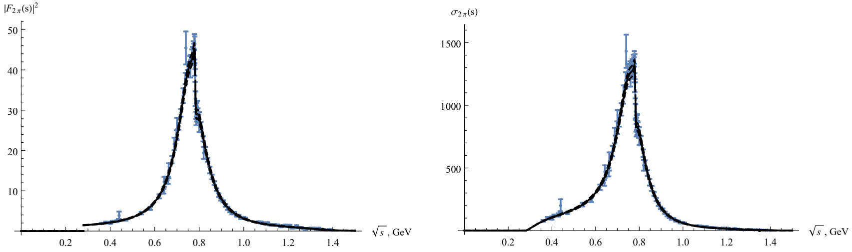

Fig.: Experimental and analytical dependencies of squared pion form factor (left), of cross section (right) on the energy for the process $e^+e^- \to \pi^+\pi^-$, $\chi^2 = 1.05$.

Data is taken from CMD and OLYA detectors[2].

[2] L. M. Barkov et al. Nucl. Phys. B256, 365–384 (1985).

Fitting. Results.

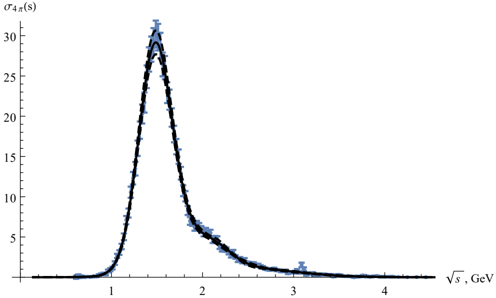

Fig.: Experimental and analytical dependencies of cross section on the energy for the process $e^+e^- \to 2\pi^+2\pi^-$, $\chi^2 = 1.85$. The fitting functions are taken as the sum of three Gaussian curves.

Data for $e^+e^- \to 2\pi^+2\pi^-$ is taken from BaBar[3].

[3] B. Aubert et al. (BABAR Collaboration) Phys. Rev. D 71, 052001 (2005).

Fitting. Results.

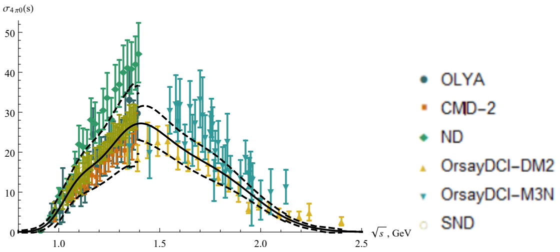

Fig.: Experimental and analytical dependencies of cross section on the energy for the process $e^+e^- \to \pi^+\pi^-2\pi^0$, $\chi^2 = 8.45$.

Data for $e^+e^- \to \pi^+\pi^-2\pi^0$ is taken from[4].

[4] M. R. Whalley. J. Phys. G: Nucl. Part. Phys. 29,A1-A133 (2003), OLYA: L. M. Kurdadze et al. J. Exp. Theor. Phys. Lett. 43, 643-645 (1986), CMD2: R. R. Akhmetshin et al. Phys. Lett. B466, 392-402 (1999), ND: Dolinsky et al. , Phys. Rep. 202(1991) 99, OrsayDCI-DM2: B. Bisello et al. Preprint LAL-90-35 (1990), OrsayDCI-M3N: G. Cosme et al. Nucl. Phys. B152, 215 (1979), SND:

Fitting. Results.

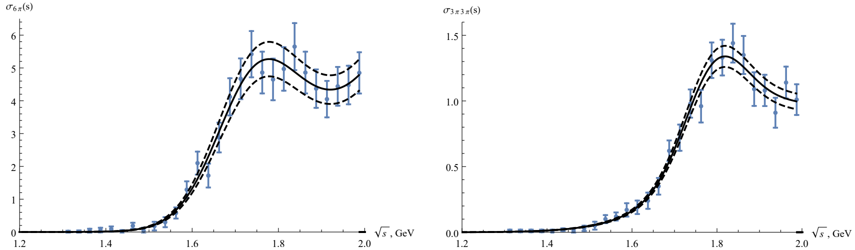

Fig.: Experimental and analytical dependencies of cross section on the energy for the processes $e^+e^- \to 3\pi^+3\pi^-$ (left), $\chi^2 = 0.62$, $e^+e^- \to 2\pi^+2\pi^-2\pi^0$ (right), $\chi^2 = 1.03$. The fitting functions are taken as the sum of three Gaussian curves.

Data is taken from BaBar [5].

[5] B. Aubert et al. Phys. Rev. D73, 052003 (2006).

Fitting. Results.

Таблица: The fitting results for particular e^+e^--annihilation channels

$e^+e^- \to \pi^+\pi^-$	V	M_V, GeV	Γ_V, GeV	α_V
$\chi^2_{\mathrm{b.f.}} = 1.05$	ρ	**0.775 (PDG)**	0.148 ± 0.006	1
	ω	**0.782 (PDG)**	**0.008 (PDG)**	0.002 ± 0.001
	ρ'	1.353 ± 0.100	0.328 ± 0.149	-0.085 ∓ 0.019

$d = 0.408 \pm 0.151$

Data from PDG:

$m_\rho = 0.77526 \pm 0.00025$ GeV;

$\Gamma_\rho = 0.1491 \pm 0.0008$ GeV;

$m_\omega = 0.78265 \pm 0.00012$ GeV;

$\Gamma_\omega = 0.00849 \pm 0.00008$ GeV;

Fitting. Results.

Таблица: The fitting results for particular e^+e^--annihilation channels

$e^+e^- \to 2\pi^+2\pi^-$	i	M_i, GeV	σ_i, GeV	α_i
$\chi^2_{\text{b.f.}} = 1.85$	1	1.512 ± 0.013	0.242 ± 0.010	1.560 ± 0.059
	2	2.125 ± 0.057	0.231 ± 0.047	0.458 ± 0.081
	3	2.656 ± 0.090	0.808 ± 0.069	0.590 ± 0.051
$e^+e^- \to \pi^+\pi^-2\pi^0$	i	M_i, GeV	σ_i, GeV	α_i
$\chi^2_{\text{b.f.}} = 8.45$	1	1.786 ± 0.018	0.327 ± 0.012	1.484 ± 0.109
	2	1.070 ± 0.025	0.099 ± 0.020	0.370 ± 0.065
	3	1.343 ± 0.017	0.188 ± 0.016	0.916 ± 0.044

Fitting. Results.

Таблица: The fitting results for particular e^+e^--annihilation channels

$e^+e^- \to 3\pi^+3\pi^-$	i	M_i, GeV	σ_i, GeV	α_i
	1	1.789 ± 0.027	0.083 ± 0.022	0.154 ± 0.035
$\chi^2_{\text{b.f.}} = 0.62$	2	2.050 ± 0.025	0.291 ± 0.020	0.433 ± 0.030
$e^+e^- \to 2\pi^+2\pi^-2\pi^0$	i	M_i, GeV	σ_i, GeV	α_i
	1	2.348 ± 0.020	0.331 ± 0.013	1.598 ± 0.140
$\chi^2_{\text{b.f.}} = 1.03$	2	1.740 ± 0.018	0.120 ± 0.015	0.558 ± 0.058

R-ratio

By definition R-ratio is:

$$R(s) = \frac{\sigma_{e^+e^- \to \mathrm{hadrons}}(s)}{\sigma_{e^+e^- \to \mu^+\mu^-}(s)}.$$

The full R-ratio is equal to the sum of R-ratios of particular channels.
At $s \leq s_0$ we use $R(s)$, obtained using experimental data, and at $s > s_0$ we use the theoretical form.

R-ratio

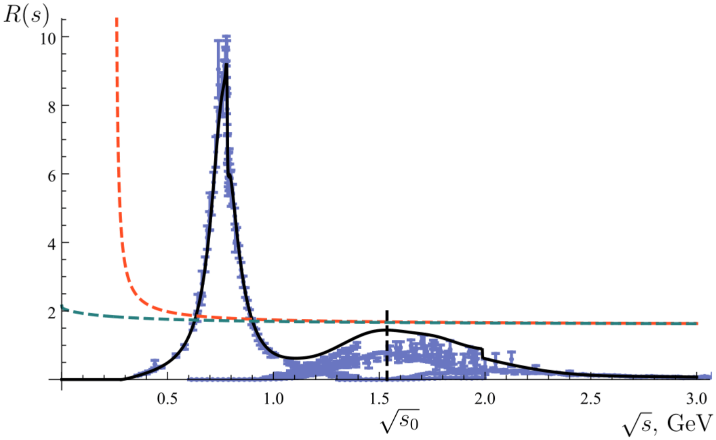

Fig.: The full R-ratio (R_{exp}) in dependence on energy $\sqrt{s}$ at $\sqrt{s} \leq 3$ GeV (black), the experimental data (blue) and the theoretical representation $R_{\text{th}}(s)$ (red).
$s_0 \approx 1.54^2$ GeV^2.

PT and APT

In ordinary Perturbaton Theory (PT) the non-physical pole (Landau-pole) exists because $\ln(Q^2/\Lambda^2)$ has singularity in $Q = \Lambda$, and running coupling has the form:

$$\alpha_s(Q^2) = \frac{4\pi}{b_0} \frac{1}{\ln(Q^2/\Lambda^2)}.$$

In Analytical Perturbaton Theory (APT) (Shirkov, Solovtsov) the coupling contains an additional term, excluding the pole:

$$\mathcal{A}_s(Q^2) = \frac{4\pi}{b_0} \left[\frac{1}{\ln(Q^2/\Lambda^2)} - \frac{\Lambda^2}{Q^2 - \Lambda^2} \right].$$

PT and APT

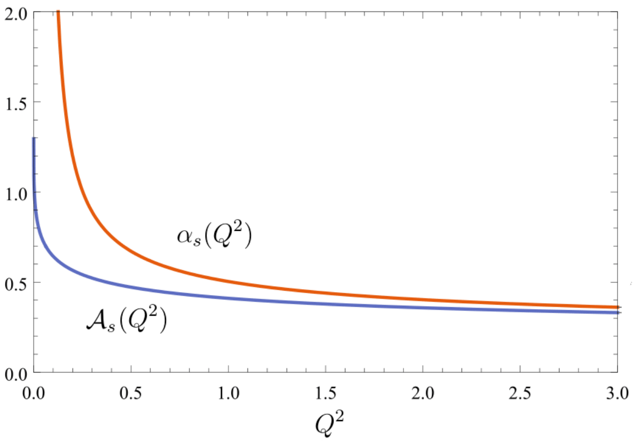

Fig.: The ordinary (orange) and analytical (blue) running couplings in dependence on energy $\sqrt{s}$ at $\sqrt{s} \leq 3$ GeV

D-function

Adler function (D-function). The dispersion relation for D-function:

$$D_{\text{Disp}}(Q^2) = Q^2 \int_0^\infty \frac{R_{\text{exp-th}}(s)\ ds}{(s+Q^2)^2}$$

$$R_{\text{exp-th}}(s) = R_{\text{exp}}(s)\,\theta(s < s_0) + R_{\text{th}}(s)\,\theta(s > s_0)\,.$$

The operator product expansion (OPE):

$$D_{\text{PT+OPE}}(Q^2) = N_c \sum_q e_q^2 \left[1 + \frac{\alpha_s(Q^2)}{\pi} + \sum_{n\geq 1} \Gamma(n)\, \frac{c_n}{Q^{2n}} \right],$$

$$D_{\text{APT+OPE}}(Q^2) = N_c \sum_q e_q^2 \left[1 + \frac{\mathcal{A}_s(Q^2)}{\pi} + \sum_{n\geq 1} \Gamma(n)\, \frac{\tilde{c}_n}{Q^{2n}} \right], N_c = 3.$$

The Borel transform. Sum rules.

$$\Phi(M^2) \;=\; \hat{B}_{Q^2\to M^2}[D(Q^2)] = \lim_{n\to\infty} \frac{(-Q^2)^n}{\Gamma(n)} \left[\frac{d^n}{dQ^{2n}} D(Q^2)\right]_{Q^2=nM^2}$$

The Borel transform is applied to the both forms of $D(Q^2)$:

$$\Phi_{\text{exp-th}}(M^2) = \int_0^\infty R_{\text{exp-th}}(s) \left(1 - \frac{s}{M^2}\right) e^{-s/M^2} \frac{ds}{M^2},$$

$$\Phi_{\text{PT+OPE}}(M^2) = \frac{3}{2} \left\{ \hat{B}_{Q^2\to M^2}\left[\frac{\alpha_s(Q^2)}{\pi}\right] + \frac{C_2}{M^2} + \frac{C_4}{M^4} + \frac{C_6}{M^6} \right\},$$

$$\Phi_{\text{APT+OPE}}(M^2) = \frac{3}{2} \left\{ \hat{B}_{Q^2\to M^2}\left[\frac{\mathcal{A}_s(Q^2)}{\pi}\right] + \frac{\widetilde{C}_2}{M^2} + \frac{\widetilde{C}_4}{M^4} + \frac{\widetilde{C}_6}{M^6} \right\}.$$

The sum rules are:

$$\Phi_{\text{PT+OPE}}(M^2) = \Phi_{\text{exp-th}}(M^2), \quad \Phi_{\text{APT+OPE}}(M^2) = \Phi_{\text{exp-th}}(M^2).$$

The Borel transform. Sum rules.

The construction of the D-function using the data and subsequent application of the Borel transform leads to the **double smearing** of the data.

That method excludes the leading term in perturbative part (the Born contribution) in R-ratio, which is important in usual applications of QCD sum rules allowing one to observe the quark-hadron duality and get the accurate description of the properties of hadrons. At the same time, that method allows one to extract non-perturbative corrections (including that due to short strings) more accurately.

Results: PT, $\Lambda = 0.25$ GeV

TABLE III: The fitting results for different intervals of M^2 in the PT, statistical errors are only in χ^2, $\Lambda = 0.25$ GeV. In the fifth column the σ-level where $C_2 = 0$ is shown. In the sixth column the (anti)correlation between gluon condensate (g.c) and C_2, g.c.(GeV^4) = A(GeV^2) $\cdot$ C_2(GeV^2) + B(GeV^4), is shown.

Range of M^2, GeV	C_2, GeV^2	$\frac{<\alpha_s GG>}{\pi}$, GeV^4	χ^2	σ-level	(Anti)correlation
[10/20, 160/20]	-0.093 $\mp$ 0.054	0.025 $\pm$ 0.008	0.758	3	$-0.153\,C_2 + 0.011$
[11/20, 120/20]	-0.076 $\mp$ 0.052	0.023 $\pm$ 0.008	0.553	3	$-0.154\,C_2 + 0.011$
[12/20, 100/20]	-0.065 $\mp$ 0.052	0.021 $\pm$ 0.008	0.406	2	$-0.154\,C_2 + 0.011$
[13/20, 90/20]	-0.058 $\mp$ 0.053	0.020 $\pm$ 0.008	0.323	2	$-0.154\,C_2 + 0.011$
[14/20, 80/20]	-0.052 $\mp$ 0.053	0.019 $\pm$ 0.008	0.265	1	$-0.155\,C_2 + 0.011$
[15/20, 70/20]	-0.047 $\mp$ 0.052	0.018 $\pm$ 0.008	0.212	1	$-0.155\,C_2 + 0.011$
[16/20, 60/20]	-0.042 $\mp$ 0.051	0.017 $\pm$ 0.008	0.156	1	$-0.155\,C_2 + 0.011$
[17/20, 50/20]	-0.037 $\mp$ 0.048	0.016 $\pm$ 0.007	0.097	1	$-0.156\,C_2 + 0.011$
[18/20, 40/20]	-0.032 $\mp$ 0.044	0.016 $\pm$ 0.007	0.041	1	$-0.156\,C_2 + 0.011$
[19/20, 30/20]	-0.027 $\mp$ 0.036	0.015 $\pm$ 0.006	0.005	1	$-0.156\,C_2 + 0.011$

Fig.: The fitting results for different intervals of M^2 in PT, $\Lambda = 0.25$ GeV

Results: APT, $\Lambda = 0.25$ GeV

TABLE IV: The fitting results for different intervals of M^2 in the APT, statistical errors are only in χ^2, $\Lambda = 0.25$ GeV. In the fifth column the σ-level where $C_2 = 0$ is shown. In the sixth column the (anti)correlation between gluon condensate (g.c) and C_2, G.c.$(\text{GeV}^4) = A(\text{GeV}^2) \cdot C_2(\text{GeV}^2) + B(\text{GeV}^4)$, is shown.

Range of M^2, GeV	C_2, GeV^2	$\frac{<\alpha_s GG>}{\pi}$, GeV^4	χ^2	σ-level	(Anti)correlation
[10/20, 160/20]	-0.067 $\mp$ 0.053	0.026 $\pm$ 0.008	0.723	2	$-0.159\,C_2 + 0.016$
[11/20, 120/20]	-0.048 $\mp$ 0.053	0.023 $\pm$ 0.008	0.508	1	$-0.159\,C_2 + 0.016$
[12/20, 100/20]	-0.036 $\mp$ 0.054	0.021 $\pm$ 0.009	0.368	1	$-0.159\,C_2 + 0.016$
[13/20, 90/20]	-0.028 $\mp$ 0.057	0.020 $\pm$ 0.009	0.296	1	$-0.159\,C_2 + 0.016$
[14/20, 80/20]	-0.022 $\mp$ 0.058	0.019 $\pm$ 0.009	0.244	1	$-0.159\,C_2 + 0.016$
[15/20, 70/20]	-0.017 $\mp$ 0.059	0.018 $\pm$ 0.009	0.195	1	$-0.159\,C_2 + 0.016$
[16/20, 60/20]	-0.012 $\mp$ 0.058	0.017 $\pm$ 0.009	0.142	1	$-0.159\,C_2 + 0.016$
[17/20, 50/20]	-0.006 $\mp$ 0.055	0.017 $\pm$ 0.009	0.086	1	$-0.160\,C_2 + 0.016$
[18/20, 40/20]	-0.000 $\mp$ 0.051	0.016 $\pm$ 0.008	0.035	1	$-0.160\,C_2 + 0.016$
[19/20, 30/20]	0.006 $\mp$ 0.045	0.015 $\pm$ 0.007	0.004	1	$-0.160\,C_2 + 0.016$

Fig.: The fitting results for different intervals of M^2 in APT, $\Lambda = 0.25$ GeV

Results: Results: PT vs APT, $\Lambda = 0.25$ GeV

The regions $\chi^2 \leq \chi^2_{\min} + 1$, $\chi^2 \leq \chi^2_{\min} + 2$ and $\chi^2 \leq \chi^2_{\min} + 3$ and the regions of existing data on gluon condensate (horizontal lines).

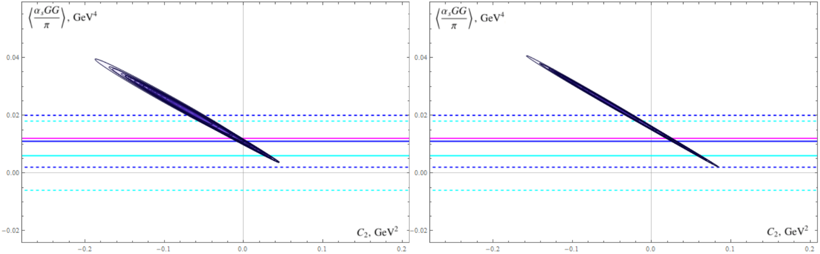

Fig.: Regions for PT (left), APT (right), $\Lambda = 0.25$ GeV. The different ellipses are for different ranges on M^2

Results: Results: PT vs APT, $\Lambda = 0.35$ GeV

The regions $\chi^2 \leq \chi^2_{\text{min}} + 1$, $\chi^2 \leq \chi^2_{\text{min}} + 2$ and $\chi^2 \leq \chi^2_{\text{min}} + 3$ and the regions of existing data on gluon condensate (horizontal lines).

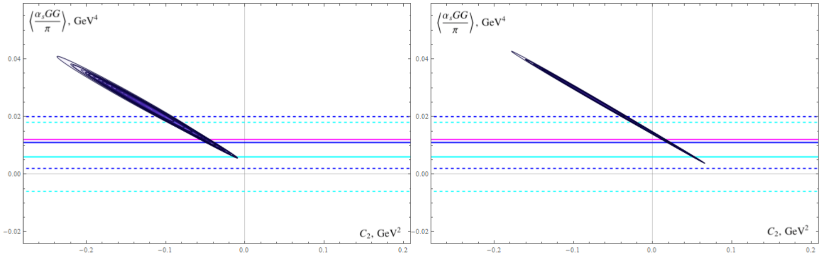

Fig.: Regions for PT (left), APT (right), $\Lambda = 0.35$ GeV. The different ellipses are for different ranges on M^2

Results: Results: PT vs APT, $\Lambda = 0.45$ GeV

The regions $\chi^2 \leq \chi^2_{\min} + 1$, $\chi^2 \leq \chi^2_{\min} + 2$ and $\chi^2 \leq \chi^2_{\min} + 3$ and the regions of existing data on gluon condensate (horizontal lines).

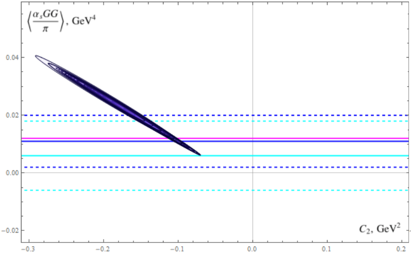

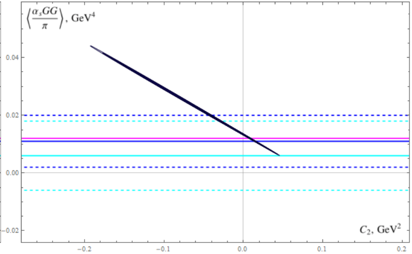

Fig.: Regions for PT (left), APT (right), $\Lambda = 0.45$ GeV. The different ellipses are for different ranges on M^2

Analysis

- A new analysis is performed. C_2 has negative sign and its compatibility to zero depends on the interval of M^2 , value of Λ and may happen only for lowest values of local gluon condensate. Dimension 2 operator is more close to zero for APT.
- (Anti)Corellation between short strings and local gluon condensate is found.
- We changed Λ and take valued 0.25 GeV, 0.35 GeV and 0.45 GeV. The C_2 region is shifted from zero to negative values more at larger Λ.

Conclusions

- The resonance contribution fitting model is developed, the Adler function with Borelization is obtained. Double smearing of the data - D-function and Borel transform.
- **Short string strongly depends on gluon condensate.** The range of M^2 is varied. At different ranges of of M^2 there are a bit different results of C_2 and gluon condensate, however the properties are common - (anti)corellation between C_2 and gluon condensate.
- **Short string also depends on choice of either standard (PT) or modified (APT) pQCD.** The APT results are shifted towards zero of C_2 in comparison with PT results. APT make results more similar to well-known.

Thank you for your attention!